ELSEVIER

Nuclear Instruments and Methods in Physics Research A 438 (1999) 253–264

NUCLEAR INSTRUMENTS & METHODS IN PHYSICS RESEARCH Section A

www.elsevier.nl/locate/nima

Photoneutron target development for the RPI linear accelerator

M.E. Overberg[1], B.E. Moretti[2], R.E. Slovacek, R.C. Block*

Gaerttner LINAC Laboratory, Department of Environmental & Energy Engineering, Rensselaer Polytechnic Institute, Troy, NY 12180-3590, USA

Received 26 February 1999; received in revised form 22 July 1999; accepted 12 August 1999

Abstract

Two new photoneutron targets have been developed for neutron time-of-flight experiments, the axial water-moderated target (AWMT) and the bare bounce target (BBT). These targets operate without any lead shielding nearby and both have superior neutron resolution compared to the older bounce target. The BBT has been selected over the AWMT for general time-of-flight measurements because it exhibited lower neutron background in the keV energy region.

1. Introduction

At the Rensselaer Polytechnic Institute Gaerttner LINAC Laboratory, transmission, capture, self-indication and scattering measurements are conducted using the neutron time-of-flight method. These measurements use the electron linear accelerator (linac) to obtain a 60 MeV electron beam incident on a tantalum target that can produce an evaporation spectrum of neutrons which peaks near 1 MeV by the $(e^- \rightarrow \gamma)$, $(\gamma \rightarrow n)$ sequence of reactions. These reactions are caused by electrons striking a set of water-cooled tantalum plates. The photoneutrons are subsequently moderated by hydrogenous material (water or polyethylene) and then travel down a series of collimated flight tubes towards the samples on the sample changer and the Li-glass detector. The resulting neutron beam allows the determination of neutron cross sections and resonance parameters through transmission, capture, self-indication or scattering experiments. Fig. 1 shows the experimental setup for transmission measurements with the 25 m flight path.

The characteristics of the tantalum target used with the linac have profound implications both for the quality of the data gathered during an experiment, and the ability to determine accurately resonance parameters from that data. Of great importance is the target resolution, which is the spread in time of the emerging neutrons (of a given energy) due to the moderating process. The current target used in linac experiments in the epi-thermal range, named the bounce target, contains a permanently attached lead personnel safety shield as part of the design. Neutron scattering by the lead in addition to the target moderator material was thought to create a 'tail' of neutrons emitted over an extended time period relative to the linac pulse width. This tail-in-time of neutrons from the bounce target was suspected to be the cause of

* Corresponding author. Tel.: +1-518-276-6404; fax: +1-518-276-4007.

[1] Now at the University of Florida, Gainesville, FL, USA.

[2] Now at the U.S. Military Academy, West Point, New York, USA.

0168-9002/99/$ - see front matter
PII: S0168-9002(99)00878-5

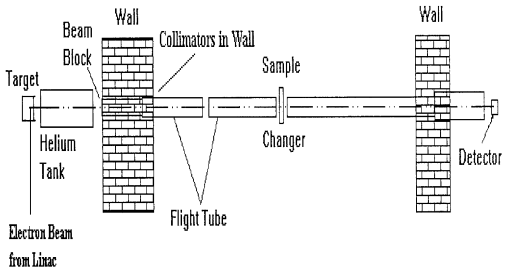

Fig. 1. Sketch of the linac 25 m flight path for transmission measurements.

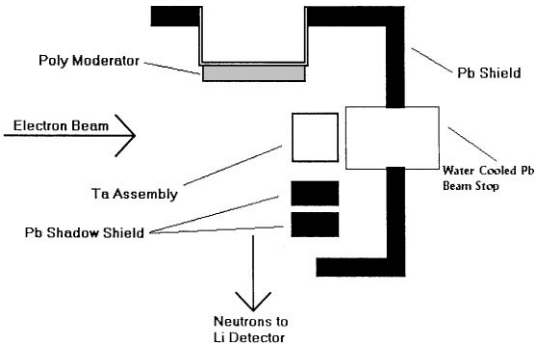

Fig. 2. Bounce target plan view.

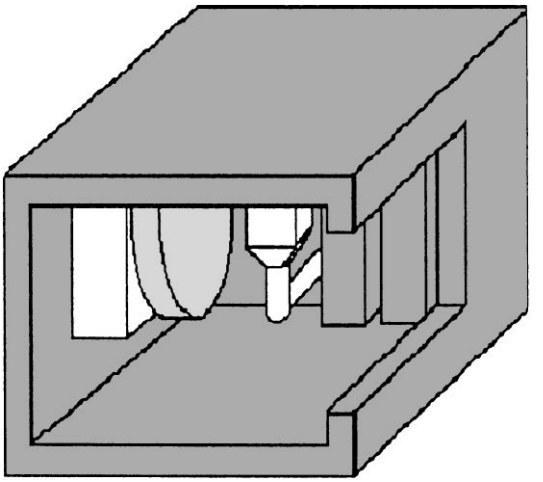

Fig. 3. The bounce target (dark gray = lead, white = aluminum, light gray = poly).

resonance distortions exhibited in the experimental data, so the modeling and construction of new targets with enhanced resolution was undertaken.

2. The bounce target

The bounce target arrangement, shown in Figs. 2 and 3 , has been used successfully at RPI for over 30 years and has proven to be a reliable target [1]. It, however, was known to be inherently deficient for several reasons. The cooling water flowing between the tantalum plates moderates some neutrons so this target has, in effect, two moderators. These neutrons slowed by collisions in the water take time to get to the polyethylene (poly) moderator where they can be further moderated and subsequently emitted down the flight path. This effect adds additional time to the overall moderation process and distorts the expected neutron time spectrum from the face of the moderator. Instead of a tightly grouped (in time) burst of like-energy neutrons leaving the moderator face, there is now a time spread in these neutrons as a result of the travel of these slower (already moderated) neutrons from the target. This time spectrum of neutrons leaving the moderator is a measure of the target resolution and significantly affects the determination of accurate experimental resonance parameters. This effect leads to a higher off-energy background and a distortion of the experimental resonance shape; both are undesirable effects.

Fig. 4 shows the neutron transmission of a 30-mil (1 mil = 0.001″ = 0.0254 mm) depleted uranium metal sample measured at the 25 m flight station and using the bounce target (see Ref. [1] for a description of this apparatus). The 6.67 eV ^{238}U resonance shape should be flat all across the bottom of the blacked-out region indicating that there is zero transmission through the 30-mil sample at this resonance energy. Instead, there is a distortion to the expected resonance shape, as indicated in Fig. 4 by the arrow. This distortion is attributed to the bounce target resolution. At higher energies the resolution distortion becomes even more prominent.

3. MCNP modeling of the bounce target

The first step in designing a new target was to model the current bounce target with the

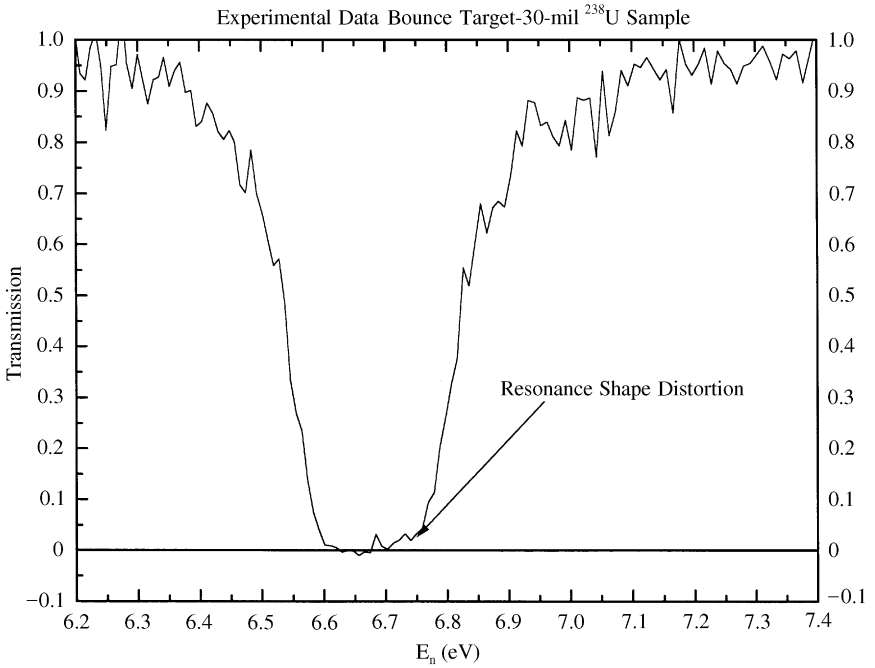

Fig. 4. Resonance shape distortion in bounce target data near the 6.67 eV resonance in ^{238}U.

neutron–photon Monte Carlo code MCNP [2] and attempt to quantify the resolution function. Through the use of MCNP statistical sampling techniques, the neutron distribution in time and energy from the face of the moderator was determined. This process resulted in the identification of the shortcomings of the bounce target and provided a method to initially validate the design of the new target.

Following the work of Danon [3,4], who also modeled the bounce target, a source term $\phi(E)$ for the tantalum plates in the target was chosen to be an evaporation energy spectrum. This has the form

$$\phi(E) = CE \exp(-E/T) \tag{1}$$

where E is the neutron energy in MeV, T is the effective temperature of the tantalum target in MeV [5,6], and C is a normalizing constant:

$$\int_0^\infty \phi(E)\,\mathrm{d}E = 1. \tag{2}$$

Using an effective temperature of 0.46 MeV, Eq. (1) produces a mean neutron energy of 0.92 MeV for the source neutrons. The source parameters were chosen such that the neutrons at "birth" are distributed uniformly throughout a homogenized mixture of tantalum and cooling water. Various time and energy bins were selected allowing an accurate determination of the target resolution function at several energies of interest. The MCNP calculations were carried out on a Sun workstation using 18 million source particles.

MCNP modeling highlighted an unexpected deficiency in the bounce target. When this target was modeled, the neutron time distribution from the target was found to have a shape that was different from that initially expected. It was expected that when a spectrum of like-energy neutrons leaving the moderator face versus time was plotted, it would approximate a Gaussian distribution or possibly a chi-square distribution, as found by Coceva and Siminoni [7] with the Oak Ridge National Laboratory's ORELA target. The result showed that the calculated distribution for the bounce target, though somewhat similar to a chi-square

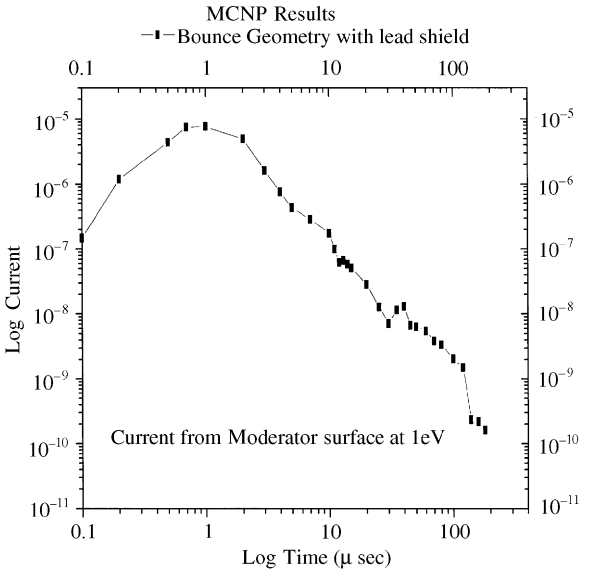

Fig. 5. Time distribution of 1 eV neutrons showing the tail-in-time from the bounce moderator surface (poly).

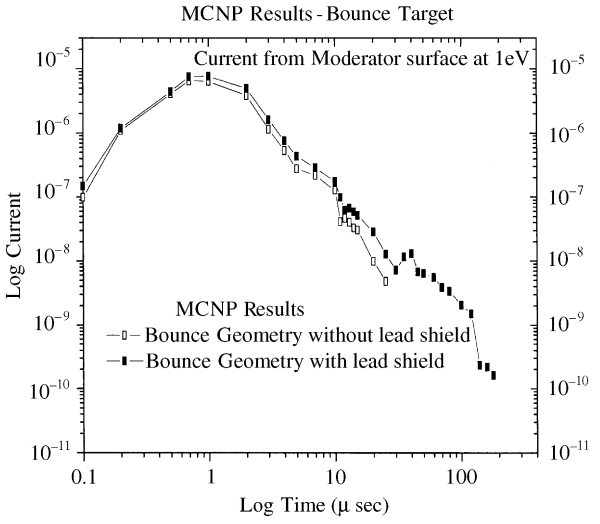

Fig. 6. The neutron distribution of 1 eV neutrons from the bounce moderator (poly) surface with the lead shield in place and with the lead shield voided.

distribution, also had a tail of neutrons extending out in time. Fig. 5 shows the calculated time distribution of 1 eV neutrons leaving the face (on the neutron detector side) of the polyethylene moderator. As expected, there is the initial large pulse of 1 eV neutrons leaving the moderator face. However, in addition to this expected neutron pulse, there is also a small tail of neutrons extending far out in time. The number of neutrons which comprise this tail is only a small percentage of the total neutrons emitted (2–5%) over the eV to keV energy ranges sampled. This resolution tail was suspected to contribute to the distortions in the blacked out resonance shapes seen in the experimental data.

MCNP runs were made in an attempt to determine the source of this tail-in-time of neutrons. Different components of the bounce target could be selectively removed by simply voiding the material card entry corresponding to that component. By using this method, the lead shield surrounding the bounce target was found to be the major source of the tail-in-time of neutrons. When the lead shield was removed, the tail-in-time of neutrons was significantly reduced. In Fig. 6, the neutron spectrum with the lead shield in place is wider and has a somewhat greater intensity than the spectrum without the shield, the result of neutrons scattering back into the moderator from the lead. The calculated spectrum without the shield shows no data point after 20 μs. The probability of a neutron being scored in a time bin greater than 20 μs had fallen off nearly three orders of magnitude, and is thus no longer statistically significant.

The scattering from the lead shield was the major cause of the tail-in-time of neutrons. Neutrons, born in the tantalum plates or escaping the water and poly moderators, were striking the shield, which nearly surrounds the bounce target. Collisions with the heavy lead nuclei resulted in very small energy losses for the neutrons. Therefore, these still energetic but now once-moderated, and subsequently delayed, neutrons reenter the poly moderator, slow down, and can be emitted down the flight tube. This tail effect was observed in every MCNP run done for this bounce target and is observed at neutron energies from 1 eV to 1 keV.

4. New target designs

An axial water-moderated target (AWMT) was designed as an on-axis target, which we define as

the tantalum assembly on the neutron beam axis. The AWMT has a similar design to the photoneutron target used at the Oak Ridge ORELA laboratory [7]. The final design was achieved using MCNP modeling with Figure-of-Merit (FOM) techniques [8,9]. To remove the resolution function broadening effects associated with a displaced moderator (as in the bounce target), the cooling water was chosen to also act as the moderator. The best FOM resulted in a water moderator with a radius of 8.89 cm and a thickness of 5.1 cm. The AWMT is shown on the left side in Figs. 7 and 8. The target consists of 10 tantalum plates separated by 1.6 mm aluminum spacers.

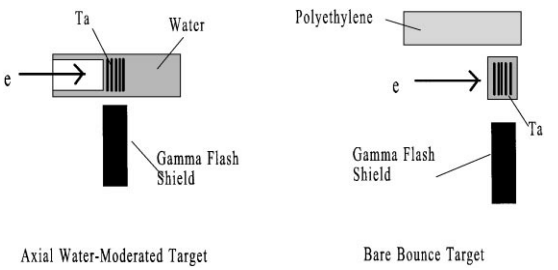

Fig. 7. Plan view of the axial water-moderated target (AWMT) and bare bounce target (BBT). For both targets a 5-cm-thick lead retractable shield (not shown) can be moved to surround the target.

The AWMT also contains an internal water baffling system to distribute the water flow. The target is constructed entirely of 6061 aluminum. The design also contains a retractable lead safety shield that surrounds the target when it is not being used. This shield is interlocked to the accelerator system so that it must be in the open position to turn the electron beam on. The shield is normally closed when people are working in the target room. For detector electronics overload protection, a 6.68 cm × 5.72 cm × 17.78 cm lead shadow shield is placed in line between the tantalum and the detector. A 5.04 cm × 5.04 cm × 1.27 cm $^{10}B_4C$ tile is attached to the side of the shadow shield that faces the tantalum to reduce neutron scattering by the lead back into the water moderator.

The bare bounce target (BBT) was designed as an adjustable target, meaning that the tantalum can be put in either an on-axis position (relative to the flight tube axis), like the AWMT, or in an off-axis position, which is displaced relative to the flight tube. In the off-axis position, the BBT has the same tantalum and polyethylene arrangement as the bounce target. The BBT has the advantage of a removable lead safety shield, also interlocked, as with the AWMT design. The BBT is shown on the right side in Figs. 7 and 8. A 17.78 cm diameter, 2.54 cm thick polyethylene disk serves as the neutron moderator. The BBT was designed to minimize the

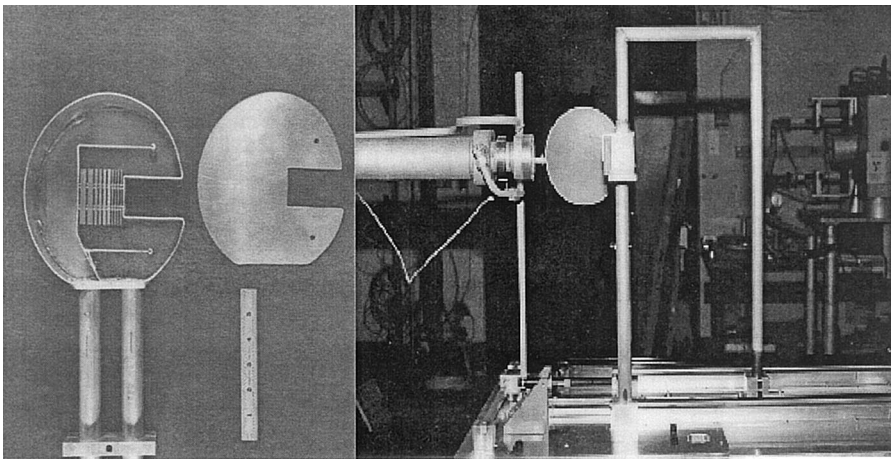

Fig. 8. The two new epi-thermal targets — the AWMT, showing the internal baffle system (left); and the BBT (in the off-axis position), showing the poly moderator with the lead safety shield retracted (to the right).

amount of cooling water in the active area of the target in order to remove as much of the second moderator as possible. The spacing between the 10 tantalum plates was reduced to 0.79 mm, and the upper and lower water plenums (for flow distribution) were reduced from a height of 5.24 to 2.54 cm. The active portion of the target (minus the cooling pipes) visible in the right side of Fig. 8 is 5.72 cm × 5.08 cm × 10.80 cm. The BBT is also entirely constructed from 6061 aluminum. Finally, it utilizes an adjustable lead shadow shield for electronics protection, and a $^{10}B_4C$ absorber on the side of the shadow shield facing the moderator.

5. Intensity increase

Experiments conducted with the AWMT and the BBT were performed to measure their neutron intensity relative to the bounce target. MCNP modeling of the AWMT predicted an increase in intensity over the bounce target [9]. For the AWMT testing, a 30 mil (0.076 cm) U depleted sample was used for both the AWMT and bounce target. To test the BBT in both the on-axis and off-axis positions relative to the bounce target, open beam data were used. For each experiment, the linac conditions were kept the same. For example, when testing the AWMT, the preset linac triggers were the same for the AWMT and the bounce target, and the machine was tuned so that the electron beam energies and currents were equal.

Results for these measurements are given in Table 1 where the errors are in standard deviations. These measurements are relative to the bounce target for a particular region of channels (the energy of the center channel for each region is given). For the AWMT, the intensity is increased on average by nearly a factor of 2.5. Clearly, the AWMT moderates a greater number of neutrons than either the bounce target or the BBT in the on-axis position. Thus, the AWMT provides the greater neutron intensity for experimental use.

The intensity of the BBT in the off-axis position is approximately equal to that from the bounce target for the entire epithermal energy range. This is not surprising, since the alignment and design of the BBT in the off-axis position is, to within a few millimeters, the same as for the bounce target. The intensity increase for the BBT in the on-axis position is not as good as that from the AWMT, but this can be attributed to the configuration of the moderating material in these targets. In the AWMT, the water moderator is on axis with respect to both the flight tube and the electron beam. In the BBT on-axis position, the poly moderator is on-axis with respect to the flight tube, but displaced with respect to the electron beam. Because of the double on-axis characteristics of the AWMT, and the fact that none of the moderator is shadowed or blocked by the tantalum itself, there is complete solid angle coupling between the AWMT and the water moderator. However, for the BBT the front surface of the poly moderator in both the on-axis and off-axis positions is almost 2.5 cm from the

Table 1
Intensity results for the BBT and the AWMT relative to the bounce target

Region (channels)	Center channel energy (eV)	AWMT	BBT (on-axis)	BBT (off-axis)
		Intensity ratio	Intensity ratio	Intensity ratio
5500–6000	4.11	2.48 ± 0.005	1.24 ± 0.003	0.98 ± 0.003
4500–5000	20.1	2.22 ± 0.002	1.30 ± 0.002	1.00 ± 0.001
3500–4000	91.2	2.26 ± 0.003	1.37 ± 0.002	1.02 ± 0.002
3000–3500	198	2.34 ± 0.003	1.41 ± 0.002	1.04 ± 0.002
2000–2500	717	2.53 ± 0.005	1.51 ± 0.004	1.06 ± 0.003
1500–2000	1200	2.64 ± 0.004	1.55 ± 0.004	1.07 ± 0.003
500–1000	6910	3.34 ± 0.005	1.79 ± 0.003	1.10 ± 0.002

electron beam axis (away from the detector), which reduces the solid angle coupling to the Ta photoneutron target. In addition, the most intense neutron source region of the poly is shielded by the tantalum itself. It may be possible to place the poly moderator in the same plane as the electron beam to increase intensity; however, care would have to be taken to avoid igniting the poly by the high-power electron beam. With the poly moderator placed on-axis with respect to both the electron beam and the detector, it would not be surprising to find that the intensity increase over the bounce target is close to that from the AWMT.

6. Signal-to-background ratio

The signal-to-background ratio was investigated using a notch1, notch2 filter package method as described by Syme [10]. The signal-to-background ratio is defined as the neutron count rate, minus background count rate, divided by the background count rate at a particular energy. It is important that this ratio is high ($\geq 10:1$) for the entire energy range of interest of the target.

Tables 2 and 3 give the results of signal-to-background measurements using open beam data and data with a U sample in the beam, respectively; errors are in standard deviations. The calculations done by Moretti [9] for both the bounce target and the AWMT are also included. As can be seen from Table 2, the signal-to-background numbers from the bounce target and the BBT in the off-axis position are approximately equal, within about two standard deviations. This result is what is expected, as the target geometries are essentially the same, except for the lead shield. However, the most encouraging result is the signal-to-background ratio obtained for the BBT in the on-axis position. The AWMT signal-to-background ratio begins to drop at the 129 eV resonance, and drops significantly at the 330 eV notch resonance. In comparison, the data for the BBT in the on-axis position suggests that the signal-to-background ratio at all of the notch resonances (except for the 2300 eV case) remains essentially constant, as opposed to gradually dropping at higher energies, as does the AWMT. In addition, the signal-to-background ratio of approximately 30 : 1 for the on-axis case is the same as for the BBT off-axis and bounce target cases. Although

Table 2
Signal-to-background measurements using open beam data

Notch energy (eV)	Bounce target (Moretti)	AWMT (Moretti)	Bounce target	BBT off-axis	BBT on-axis
5	33.1 ± 8	35.8 ± 6	24.9 ± 4.0	35.0 ± 5.6	37.6 ± 5.0
19	—	—	23.9 ± 3.3	31.4 ± 5.2	21.3 ± 2.8
129	31.6 ± 3	27.1 ± 1.3	26.6 ± 3.3	27.2 ± 3.4	31.6 ± 3.0
330	31.3 ± 2.1	17.2 ± 0.6	32.4 ± 2.8	28.7 ± 2.6	32.9 ± 2.4
2300	8.3 ± 0.3	6.4 ± 0.1	7.3 ± 0.6	8.7 ± 0.6	9.1 ± 0.5

Table 3
Signal-to-background measurements using data with a U sample in the beam

Notch energy (eV)	Bounce target (Moretti)	AWMT (Moretti)	BBT off -axis	BBT on-axis
5	33.1 ± 8	35.8 ± 6	24.3 ± 3.7	26.8 ± 3.3
19	—	—	33.2 ± 5.2	23.5 ± 2.7
129	31.6 ± 3	27.1 ± 1.3	29.5 ± 3.2	27.8 ± 2.4
330	31.3 ± 2.1	17.2 ± 0.6	29.0 ± 2.5	27.1 ± 1.7
2300	8.3 ± 0.3	6.4 ± 0.1	7.7 ± 0.5	7.7 ± 0.4

the intensity for the AWMT increases on average by a factor of 2.5, the background at higher energies increases by nearly a factor of 4.0. Through further experiments, the increased background was found to be beam associated, but no firm cause was established.

From Table 3, one can find further support for the statement made in the previous paragraph. That is, the BBT in both positions has a consistent, approximately 30 : 1 ratio for all of the notch resonance energies, except for the 2300 eV region, which is approximately 7 : 1. Thus, to enable accurate cross section measurements in the keV region, the BBT was judged superior to the AWMT. The BBT was selected as the target for epithermal measurements.

7. Resolution improvements and a quantitative resolution function

To see if the AWMT and BBT targets provide a resolution improvement over the bounce target, a series of experiments was performed in transmission (with a 30 mil depleted U sample) and capture (with a 1 mil natural U sample). These experiments were intended to show the improvement in resolution. Primarily, this experiment was done to confirm whether or not the resolution improved by removing the fixed lead shield, as predicted by the MCNP modeling.

Figs. 9–12 show the 66 and 102.5 eV ^{238}U resonances in capture and transmission. In capture, Figs. 9 and 10, the BBT shows a dramatic reduction in the amount of neutron tail compared to the bounce target seen in the low energy wing of both resonances. The two transmissions, Figs. 11 and 12, show a reduced amount of neutron tail for both the AWMT and the BBT compared to the bounce target in the low-energy wing of the resonances. The resonances are also deeper for the BBT and the AWMT than for the bounce target. This also indicates an improved resolution for the BBT and the AWMT compared to the bounce target.

To allow a quantitative comparison of the resolution of each target, an empirical method was used which involved broadening the calculated

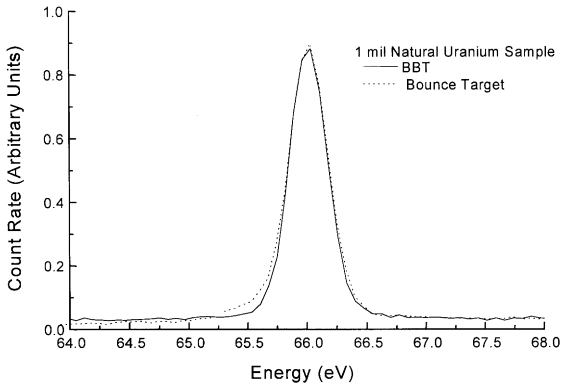

Fig. 9. Capture data near the 66 eV ^{238}U resonance for the bounce target and the BBT.

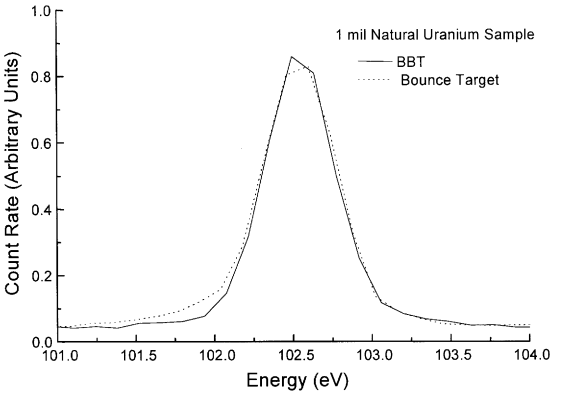

Fig. 10. Capture data near the 102.5 eV ^{238}U resonance for the bounce target and BBT.

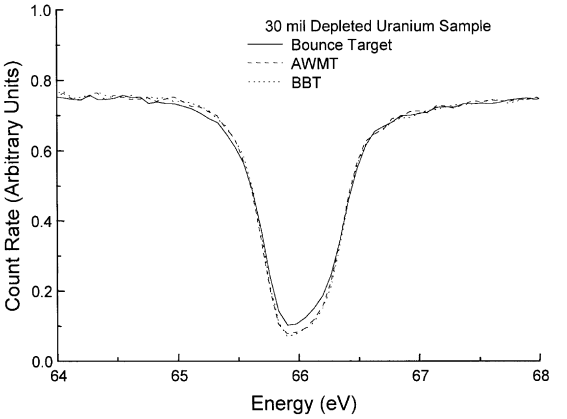

Fig. 11. Transmission data near the 66 eV ^{238}U resonance for the bounce target, the AWMT and the BBT.

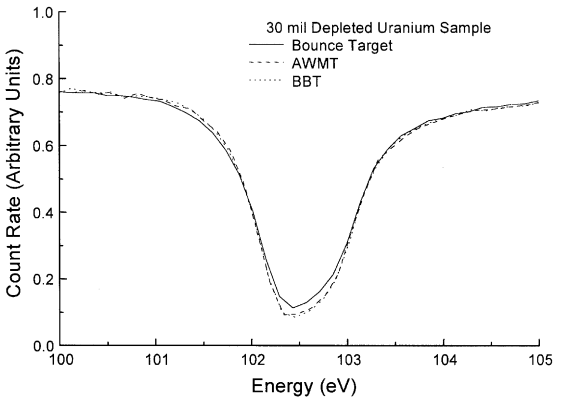

Fig. 12. Transmission data near the 102.5 eV ^{238}U resonance for the bounce target, the AWMT and the BBT.

transmission, based on ENDF/B-VI evaluated cross-section data [11] for ^{238}U. The calculated transmission was broadened with a resolution function that contained several variable parameters, and then the resolution-broadened data were compared to the experimental data. The resolution function parameters, which lead to the best fit of the experimental data, were selected to represent the RPI resolution function. Using this method and the MCNP modeling results as a guide, the target and detector resolution function for the AWMT, BBT, and bounce target were determined and compared.

The total resolution function has four components, which act to broaden the data: the burst width, the channel width, the target plus moderator, and the detector. The burst width and channel width component shapes are well known and can be described by a Gaussian and rectangular function, respectively. Pre-broadening the theoretical resonance shape with a Gaussian function, representing the burst width, and a rectangular function, representing the channel width, accounts for the broadening effects of two of the four resolution function components. Using this pre-broadening procedure, the resolution function, which achieves a best match to the experimental data, represents the target and detector resolution components only. Since the bounce target, BBT, and AWMT experimental data were gathered in transmission using the same detector, this method allows a direct comparison of the resolution performance of each target and a determination of the combined target and detector resolution function shape.

The resolution parameters could be determined at each resonance energy. Then the energy dependence of these parameters could be obtained by fitting them over this energy-range. This energy-dependent resolution function is then valid over that energy range.

Using MCNP results as a guide, a sum-of-exponentials function was added to a chi-square function to describe the tail-in-time of neutrons from the target. This sum-of-exponentials function was inferred from modeling the neutron attenuation in the ^{6}Li-glass detector using MCNP. The chi-square function was used as a starting point since it is used to describe the target resolution in SAMMY [12], an Oak Ridge code used at RPI for the determination of resonance parameters. The chi-square function used for the resolution function fitting took on the form

$$\frac{(t+\text{shift})^2}{2\Lambda^3}\exp\left[\frac{-(t+\text{shift})}{\Lambda}\right] \tag{3}$$

where the variables Λ and shift are adjustable parameters during the fitting. The non-negative neutron tail-in-time, fitted to the experimental results, took on the form

$$A_1\left[A_2\, e^{-A_3(t+t_0)} + A_4\exp\left(-\left(\frac{t+\text{shift}}{\Lambda}\right)\right)\right] \tag{4}$$

where A_1 also is an adjustable parameter to increase or decrease the amount of neutron tail. Thus, during a resolution function fit, the three parameters to adjust are Λ, shift, and A_1. For the target and Li-glass detector system, the following values have been obtained: $A_2 = -65.638$; $A_3 = 5.0$; $A_4 = 0.39383$; $t_0 = 0.94$ μs; shift = 0.94 μs; $\Lambda = 1.25$ μs.

As an example, the left side of Fig. 13 shows ENDF ^{238}U data for the 102.5 eV resonance broadened only with the burst and channel width functions, overlaid with experimental data for the AWMT with a 30 mil sample. The right side of Fig. 13 shows the same ENDF data, now broadened with all the components of the resolution function. This consists of the sum of Eqs. (3) and (4). The integral over all time of this sum is normalized to

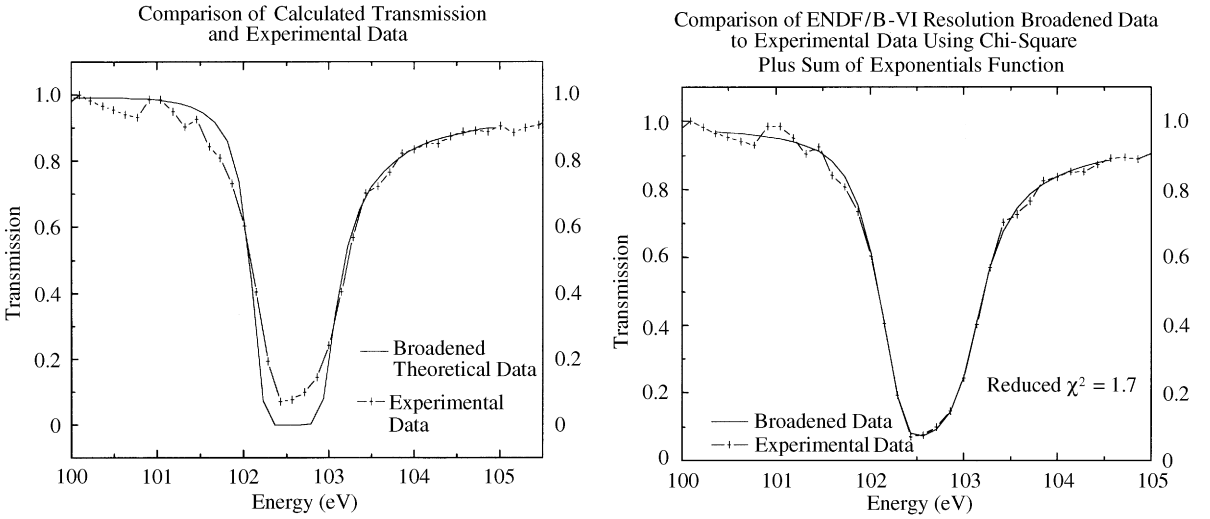

Fig. 13. ^{238}U ENDF data broadened only with the burst and channel width functions, compared with experimental data (left side); and ENDF ^{238}U data broadened with all the components of the resolution function, compared with experimental data (right side). The AWMT target was used for this experiment.

unity. This represents the best fit possible by adjusting the three independent parameters within the resolution function, based upon a calculated minimum reduced chi-square (χ^2_R). The excellent fit to the experimental data here is reflected in a low value of $\chi^2_R = 1.7$. Fig. 14 shows the resolution function providing the fit given in Fig. 13 (right side) for the AWMT, representing the combined target and detector resolution effects.

Experiments were performed for the AWMT, BBT and bounce target using U samples to evaluate the resolution function for each. The experimental data were then fitted with Eqs. (3) and (4), to determine A, shift, and A_1 [9]. The results of the fitting are presented in Tables 4 and 5 for the combined target and detector components of the resolution function. For the BBT data, the quantity in parenthesis is the thickness (in mils) for the U sample used to get that particular χ^2_R. A 30 mil sample was used in all cases for the bounce target and the AWMT, where only transmission data were obtained. Tables 4 and 5 do not provide values for the shift variable because a value for the shift variable is not indicative of the quality of the target in terms of the resolution function. Comparing the values for shift for all three targets at a particular resonance energy does not tell if one target is best; it merely brings the experimental data in temporal alignment with the burst and channel width broadened ENDF data. Note that the parameter A depends upon the moderator, target geometry, and detector geometry in a complicated manner. The chi-square value represents the result of the best fit to the experimental data.

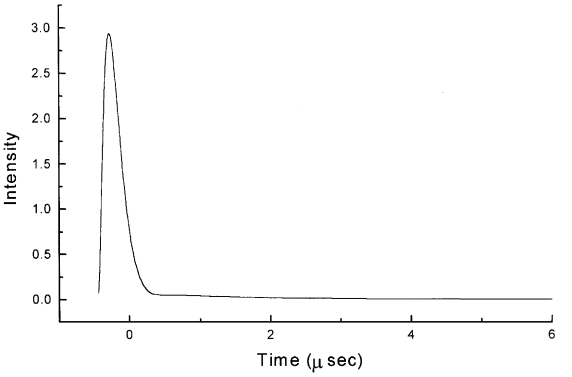

Fig. 14. Best fit resolution function for the AWMT at 102.5 eV in ^{238}U.

Tables 4 and 5 show the superiority of the new BBT and AWMT over the older bounce target.

Table 4
Values of Λ and the related χ^2_R for the BBT, bounce, and AWMT

Resonance energy (eV)	BBT Λ (μs)	BBT χ^2_R	Bounce target Λ (μs)	Bounce target χ^2_R	AWMT Λ (μs)	χ^2_R
66.03	0.101	1.1 (5) 2.1 (10)	0.114	2.1	0.100	1.4
102.54	0.085	1.1 (5) 2.6 (10) 1.3 (20)	0.096	1.7	0.085	1.7
116.9	0.083	2.6 (10) 2.1 (20)	0.093	1.7	0.082	2.1
189.7	0.073	3.9 (10) 1.3 (20)	0.086	3.4	0.074	2.4

Table 5
Values of A_1 and the related χ^2_R for the BBT, Bounce, and AWMT

Resonance energy (eV)	BBT A_1	BBT χ^2_R	Bounce target A_1	Bounce target χ^2_R	AWMT A_1	AWMT χ^2_R
66.03	0.579	1.1 (5) 2.1 (10)	0.834	2.1	0.485	1.4
102.54	0.749	1.1 (5) 2.6 (10) 1.3 (20)	0.958	1.7	0.540	1.7
116.9	0.648	2.6 (10) 2.1 (20)	0.977	1.7	0.590	2.1
189.7	0.715	3.9 (10) 1.3 (20)	1.00	3.4	0.610	2.4

From Table 4, the resolution function fits show that for every sampled ^{238}U resonance, the values for Λ are lower for the BBT and the AWMT water moderated compared to the bounce target. This lower value for Λ quantitatively proves what was seen in Figs. 9–12 in terms of resolution improvement. Table 5 also shows a reduced amount of neutron tail (A_1) for both the BBT and AWMT. This is attributed to the removal of the fixed lead shield in these target designs, and confirms the MCNP modeling results discussed previously.

8. Conclusion

Two new photoneutron targets have been developed for neutron time-of-flight experiments at the Gaerttner LINAC Laboratory. When compared to the older bounce target, both the AWMT and BBT exhibited superior resolution. The AWMT had twice the neutron intensity as the bounce target, while the BBT in the off-axis position had the same intensity as the bounce target. However, the AWMT had higher neutron background (lower signal-to-background ratio) in the keV energy region than either the BBT or the bounce target. Given the BBTs superior signal-to-background ratio in the keV energy region and its versatility to be readily configured from an off-axis to on-axis target, the BBT has been selected as the target of choice for epithermal time-of-flight measurements.

Acknowledgements

The authors thank the technical staff of the Gaerttner LINAC Laboratory for their assistance in constructing the new targets and for providing a very

smooth and efficient operation of the electron accelerator. We appreciate the assistance of Chris Werner and John Burke in getting us up to speed on the operation of the SAMMY program. Finally, we thank the members of the Cross Section Group in helping out in the running of the experiments.

References

[1] R.W. Hockenbury, Z.M. Bartolome, J.R. Tatarczuk, W.R. Moyer, R.C. Block, Phys. Rev. 178 (4) (1969) 1746.
[2] MCNP, Monte Carlo N-Particle Transport Code System, Version 4A, Los Alamos National Laboratory, LA-12625-M, 1993.
[3] Y. Danon, Design and construction of the RPI enhanced thermal neutron target and thermal cross section measurements of rare earth isotopes, Doctoral Thesis, Rensselaer Polytechnic Institute, 1993.
[4] Y. Danon, R.C. Block, R.E. Slovacek, Nucl. Instr. and Meth. A 352 (1995) 596.
[5] C.R. Stopa, Measurements of neutron induced fission cross sections of ^{244}Cm, ^{246}Cm and ^{248}Cm by means of lead slowing-down-time spectrometry, Doctoral Thesis, Rensselaer Polytechnic Institute, 1983.
[6] Gayther-Goode, UKAEA Harwell, R5331, 1966.
[7] C. Coceva, R. Simonini, Nucl. Instr. and Meth. 211 (1983) 459.
[8] A. Michaudon, J. Nucl. Sci. Technol. (J. Nucl. Energy Parts A/B) 17 (1963) 165.
[9] B. Moretti, Molybdenum neutron transmission measurements and the development of an enhanced resolution neutron target, Doctoral Thesis, Rensselaer Polytechnic Institute, 1996.
[10] D.B. Syme, Nucl. Instr. and Meth. 198 (1982) 357.
[11] ENDF/B-VI, Evaluated Nuclear Data Files, Brookhaven National Laboratory, National Nuclear Data Center, On-line data Service, 1997.
[12] N.M. Larson, SAMMY-H1: a code system for multilevel R-matrix fits to neutron data using Bayes equations, ORNL/TM-9179/R2 and Draft R3, 1994.